Toward sensorless acquisition of multiple contact points between planar parts

Kevin Egan[1], Stephen Berard[1], and Jeffrey C. Trinkle[1]

Department of Computer Science
Rensselaer Polytechnic Institute
Troy NY, 12180-3590
{ktegan, sberard, trink}@cs.rpi.edu
http://www.cs.rpi.edu/∼{ktegan, sberard, trink}

Abstract. A fixture is a device which immobilizes a part through a maximal set of linearly independent contacts. While many techniques exist to determine an appropriate arrangement of contacts, little research has been done on how to acquire those contacts (*i.e.*, move the part such that it makes contact with the fixture at all intended points). In previous work, it was assumed that the gaps between the part and the fixture were infinitesimal. This allowed the use of a continuous-time model (formulated as a linear complementarity problem) to determine a set of contact wrenches, any one of which could be applied to the part to acquire all contacts simultaneously. This set was mapped to the boundary of the part to identify a pushing region on the part where one could push with a single finger to acquire the contacts.

The work presented here provides two primary improvements. First, it is based on a discrete-time rigid body dynamics model that takes into account the finite motion of a part needed to close finite initial gaps between the part and the fixture. This model also allows one to determine a convex set of applicable wrenches. Second, a technique is developed whereby finite regions of the part's boundary can be tested for membership in the pushing region, thus eliminating the need for point-wise testing.

1 Introduction

In the planning of robot manipulation tasks involving unilateral contact(s), a task is often decomposed into a sequence of subtasks such that for each subtask, the set of contacts and their interactions (for the planar case: sliding left, sliding right, rolling, separating) are constant [1–6]. The reason for this decomposition is that the structure of the dynamic model is constant for each subtask and often the problem size can be reduced by eliminating a subset of the unknowns.

In this paper, we study the *part seating problem* in the plane. Given two bodies, one fixed (the fixture) and one moveable (the part), the initial configuration of the part relative to the fixture, and the goal configuration of the part in the fixture, determine a set of wrenches, which when applied to the part, will move it to the goal configuration. Once this set is found, we also map it to the boundary of the part to identify a pushing region where one could push the part with a single finger to seat it.

Figure 1 illustrates the part seating problem for the simple case (simple because a point of unit mass's configuration space is identical to its workspace) of seating a
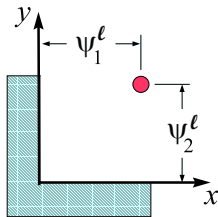
Fig. 1. Part seating example illustrating a point mass near its goal configuration, the corner. The initial position of the point is given by Ψ_1^ℓ, Ψ_2^ℓ

single point. For this example, the goal position is when the point is in the corner, touching both the x- and y-axes. Therefore, the task is to find the set of external wrenches that will drive the point of unit mass with initial position $\left(\Psi_1^\ell, \Psi_2^\ell\right)$ into the corner.

In previous work, Balkcom and Trinkle [7] analyzed the part seating problem under the assumption that the initial configuration of the part was infinitesimally close to the goal configuration ($\Psi_1^\ell = \Psi_2^\ell = 0$ from Figure 1), so that the gaps between the part and the intended contact points were negligible. These assumptions suggested the use of an instantaneous dynamic model of the system. Using the model formulated as a linear complementarity system in [8], Balkcom and Trinkle developed an algorithm that determined a polyhedral cone of wrenches each of which could be applied to seat the part.[1] This set was mapped to the boundary of the part in a brute force manner. For each sampled point on the boundary of the part, the set of wrenches that could be applied to the part through frictionless contact at that point was determined and then tested for membership in the wrench cone. If the contact wrench was in the cone, then that point was considered to be in the pushing region.

In this paper, we extend this work to take into account (nonzero) finite gaps between the part and the fixture ($\Psi_1^\ell > 0$, $\Psi_2^\ell > 0$ from Figure 1). To do this, the continuous-time model is replaced by a the semi-implicit Euler time-stepping model developed by Stewart and Trinkle [9,10]. In addition to allowing the analysis to properly account for finite gaps, the discrete-time approach eliminates the need for detailed analysis of all possible orders of contact achievement, as was required by the instantaneous analysis.

We also present a new approach for determining the pushing region on the boundary of the part. This method maps an arbitrary wrench set to the boundary of the part. It can identify the pushing region suitable for a frictionless pusher, but can also identify a smaller region for a frictional pusher (which is smaller because we require that all contact forces within the friction cone must belong to the part seating wrench cone).

---

[1] This cone of wrenches was composed of those guaranteed to seat the part despite nonuniqueness of the dynamic model.

2 Discrete-Time Dynamic Model

Since the discrete-time model takes the form of a linear complementarity problem (LCP), we define the standard linear complementarity problem here.

Definition 1. LCP(B, b), Given the constant matrix $B \in \Re^{n \times n}$ and vector $b \in \Re^n$, find vectors $w \in \Re^n$, $z \in \Re^n$ satisfying the following conditions:

$$w = Bz + b \tag{1}$$

$$0 \le w \perp z \ge 0 \tag{2}$$

where $w \perp z$ implies that w and z are perpendicular (*i.e.,* $w^T z = 0$). This LCP is said to be of size n.

Note that if the matrix B is a P-matrix (a generalization of a positive definite matrix), then the LCP has a unique solution for every b. In addition, if B is a P-matrix, then the Lemke's algorithm will find the solution with a finite number of operations [11].

2.1 Continuous-Time Dynamic Model

For clarity, we briefly describe the discretization of the continuous time model for planar multi-rigid-body systems. This model consists of the Newton-Euler equation, a velocity kinematics equation, normal complementarity conditions, and tangential complementarity conditions. Let ν and q denote the generalized velocity and configuration of a part with n_c frictional unilateral contacts. Then the Newton-Euler and rotational kinematics equations can be written as follows:

$$M\dot{\nu} = W_{\mathrm{n}}\lambda_{\mathrm{n}} + W_{\mathrm{t}}\lambda_{\mathrm{t}} + g_{\mathrm{ext}} \tag{3}$$

$$\dot{q} = \nu \tag{4}$$

where $M \in \Re^{3 \times 3}$ is the positive definite inertia matrix, $\dot{\nu} \in \Re^3$ is the generalized acceleration of the part, $\lambda_{\mathrm{n}} \in \Re^{n_c}$ is a vector of normal force components at the contacts, $\lambda_{\mathrm{t}} \in \Re^{n_c}$ vector of friction force components at the contacts, and $g_{\mathrm{ext}} \in \Re^3$ is the sum of all non-contact wrenches. The matrices W_{n}, W_{t}, and M have the following forms:

$$W_{\mathrm{n}} = \begin{bmatrix} \cdots & \hat{n}_i & \cdots \\ & r_i \otimes \hat{n}_i & \end{bmatrix} \quad W_{\mathrm{t}} = \begin{bmatrix} \cdots & \hat{t}_i & \cdots \\ & r_i \otimes \hat{t}_i & \end{bmatrix} \quad M = \begin{bmatrix} m & 0 & 0 \\ 0 & m & 0 \\ 0 & 0 & I \end{bmatrix} \tag{5}$$

where r_i is the vector from the part's center of mass to contact i, $\hat{n}_i$ is the unit normal vector pointing into the part at contact i, $\hat{t}_i$ is the unit tangent vector obtained by rotating the normal vector $\pi/2$ radians counter clockwise from the normal vector at contact i, $r_i \otimes \hat{n}_i$ is defined as $r_{ix}n_{iy} - r_{iy}n_{ix}$, m is the mass of the part, and I is the moment of inertia of the part about the axis perpendicular to the plane and containing the center of mass of the part.

   Let $\Psi_{in}(q)$ be the distance between the part and the ith intended point of contact on the fixture (the ith "fixel"). Then $\Psi_{\mathrm{n}}(q) = [\ldots \Psi_{in}(q) \ldots]^T$ is the vector of

distances between the part and fixels. The time rate of change of $\boldsymbol{\Psi}_{\mathrm{n}}(\boldsymbol{q})$ is the vector of normal components of velocity between the part and each fixel. That is:

$$\dot{\boldsymbol{\Psi}}_{\mathrm{n}}(\boldsymbol{q}) = \nabla_q \boldsymbol{\Psi}_{\mathrm{n}} \dot{\boldsymbol{q}} = \boldsymbol{W}_{\mathrm{n}}^{T} \boldsymbol{\nu}, \tag{6}$$

where ∇_q implies partial differentiation with respect to $\boldsymbol{q}$. The analogous tangential kinematic equation is:

$$\boldsymbol{v}_{\mathrm{t}} = \boldsymbol{W}_{\mathrm{t}}^{T} \boldsymbol{\nu} \tag{7}$$

It is assumed that Coulomb friction acts at the contacts. Coulomb's Law states that at a rolling contact the contact force lies in a cone. By contrast, at a sliding contact, the contact force must lie on the boundary of the cone in the direction maximizing the dissipation of energy. Coulomb's Law applied to contact i can be written as follows:

$$|\lambda_{it}| \leq \mu_{is}\lambda_{in} \qquad\qquad i \in \mathcal{R} \tag{8}$$
$$\lambda_{it} = -sign(v_{it})\mu_{ik}\lambda_{in} \quad i \in \mathcal{S} \tag{9}$$

where the index sets $\mathcal{R} = \{i \mid \Psi_{in} = v_{in} = v_{it} = 0\}$ and $\mathcal{S} = \{i \mid \Psi_{in} = v_{in} = 0; \ v_{it} \neq 0\}$ identify the rolling and sliding contacts, respectively, and μ_{is} and μ_{ik} are the static and kinetic coefficients of friction at contact i.

2.2 Conversion from a Continuous-Time to a Discrete-Time Dynamic Model

Let us assume that we have estimates of the configuration and generalized velocity at the current time t_ℓ, and assume further that the set of contacts and a set of possible future contacts is known. The goal of a time-stepping model is to estimate the configuration, generalized velocity, and contact forces at time $t_{\ell+1} = t_\ell + h$, where h is the time step. In other words, given $\boldsymbol{q}^\ell = \boldsymbol{q}(t_\ell)$ and $\boldsymbol{\nu}^\ell = \boldsymbol{\nu}(t_\ell)$ compute approximations $\boldsymbol{q}^{\ell+1} = \boldsymbol{q}(t_{\ell+1})$ and $\boldsymbol{\nu}^{\ell+1} = \boldsymbol{\nu}(t_{\ell+1})$.

The approach taken by Stewart and Trinkle [9,10] is to replace the time derivatives $\dot{\boldsymbol{\nu}}$ and $\dot{\boldsymbol{q}}$ by their backward Euler approximations ($\dot{x} \approx \frac{x^{\ell+1} - x^\ell}{h}$):

$$\boldsymbol{M}(\boldsymbol{\nu}^{\ell+1} - \boldsymbol{\nu}^\ell) = \boldsymbol{W}_{\mathrm{n}}^\ell \boldsymbol{p}_n^{\ell+1} + \boldsymbol{W}_{\mathrm{t}}^\ell \boldsymbol{p}_t^{\ell+1} + \boldsymbol{p}_{\mathrm{ext}}^\ell \tag{10}$$
$$\boldsymbol{q}^{\ell+1} - \boldsymbol{q}^\ell = h\boldsymbol{\nu}^{\ell+1}, \tag{11}$$

where $\boldsymbol{p}_n^{\ell+1} = h\boldsymbol{\lambda}_{\mathrm{n}}^{\ell+1}$, $\boldsymbol{p}_t^{\ell+1} = h\boldsymbol{\lambda}_{\mathrm{t}}^{\ell+1}$, and $\boldsymbol{p}_{\mathrm{ext}}^{\ell+1} = h\boldsymbol{w}_{\mathrm{ext}}^{\ell+1}$ are the contact and external impulses delivered to the part over the time interval $(t_\ell, \ t_{\ell+1}]$. Although these expressions appear linear in the unknowns, in general $\boldsymbol{M}, \boldsymbol{W}_{\mathrm{n}}, \boldsymbol{W}_{\mathrm{t}}$, and $\boldsymbol{p}_{\mathrm{ext}}$ depend on $\boldsymbol{q}(t)$ and $\boldsymbol{\nu}(t)$. If we assume their values are constant over the time interval $(t_\ell, t_{\ell+1})$, then we can simply evaluate them at t_ℓ. In this case, equations (10) and (11) become linear in the unknowns, which is required to formulate the time stepping problem as a *linear* complementarity problem.

2.3 Normal Complementarity

In order to achieve a time-stepping formulation that is an LCP rather than a non-linear complementarity problem (which is more difficult to solve), we linearize the nonpenetration constraints via a truncated Taylor series expansion. Recalling that the linearized constraints must be satisfied at the end of the current time step and using equations (6) and (11) one arrives at the following linear inequality:

$$\boldsymbol{\Psi}_{\mathrm{n}}^{\ell+1} = \boldsymbol{\Psi}_{\mathrm{n}}^{\ell} + h\boldsymbol{W}_{\mathrm{n}}^{T}\boldsymbol{\nu}^{\ell+1} \geq 0 \tag{12}$$

Complementarity exists between the gap $\boldsymbol{\Psi}_{\mathrm{n}}^{\ell+1}$ and the contact impulse $\boldsymbol{p}_{\mathrm{n}}^{\ell+1}$ at the end of the current time step:

$$0 \leq \boldsymbol{\Psi}_{\mathrm{n}}^{\ell} + h(\boldsymbol{W}_{\mathrm{n}}^{\ell})^{T}\boldsymbol{\nu}^{\ell+1} \perp \boldsymbol{p}_{n}^{\ell+1} \geq 0. \tag{13}$$

Physically this complementarity condition ensures that the normal component of the contact impulse can only be nonzero if contact is achieved at the end of the time step.

2.4 Tangential Complementarity

To capitalize on the tools and techniques of complementarity, we must work with nonnegative variables. Therefore we replace the friction impulse at contact i, p_{it} (which may be negative) with the sum of its positive and negative parts $(p_{if})_1 \geq 0$ and $(p_{if})_2 \geq 0$, allowing us to express the friction cone $\mathcal{F}_i$ at fixel i as follows:

$$\mathcal{F}_i(\boldsymbol{q}) = \{\, \boldsymbol{W}_{in}p_{in} + \boldsymbol{W}_{if}\boldsymbol{p}_{if} \mid p_{in} \geq 0,\ \boldsymbol{p}_{if} \geq 0,\ \boldsymbol{e}^T\boldsymbol{p}_{if} \leq \mu_i p_{in} \,\} \tag{14}$$

where $\boldsymbol{e} = [1\ \ 1]^T$ and $\boldsymbol{p}_{if}$, $\boldsymbol{W}_{in}$, and $\boldsymbol{W}_{if}$ are defined as follows:

$$\boldsymbol{p}_{if} = \begin{bmatrix} (p_{if})_1 \\ (p_{if})_2 \end{bmatrix} \qquad \boldsymbol{W}_{in} = \begin{bmatrix} \hat{\boldsymbol{n}}_i \\ \boldsymbol{r}_i \otimes \hat{\boldsymbol{n}}_i \end{bmatrix} \qquad \boldsymbol{W}_{if} = \begin{bmatrix} \hat{\boldsymbol{t}}_i & -\hat{\boldsymbol{t}}_i \\ \boldsymbol{r}_i \otimes \hat{\boldsymbol{t}}_i & -\boldsymbol{r}_i \otimes \hat{\boldsymbol{t}}_i \end{bmatrix}.$$

While the definitions just given ensure that the contact impulses remain within the friction cone, they do not enforce maximal energy dissipation at a contact when it slides. This is accomplished by introducing a slack variable s_i that is equal to the magnitude of the tangential component of the velocity of the part at contact i. When this variable is zero, then the contact impulse may lie anywhere within the friction cone, but when it is positive, the contact impulse must lie on the boundary of the friction cone in the direction that opposes the sliding motion. The Coulomb friction behavior can be captured by the following pair of linear complementarity conditions:

$$0 \leq \begin{bmatrix} \boldsymbol{\rho}_{\mathrm{f}}^{\ell+1} \\ \boldsymbol{\sigma}^{\ell+1} \end{bmatrix} = \begin{bmatrix} (\boldsymbol{W}_{\mathrm{f}}^{\ell})^{T}\boldsymbol{\nu}^{\ell+1} + \boldsymbol{E}\boldsymbol{s}^{\ell+1} \\ \boldsymbol{U}\boldsymbol{p}_{\mathrm{n}}^{\ell+1} - \boldsymbol{E}^{T}\boldsymbol{p}_{\mathrm{f}}^{\ell+1} \end{bmatrix} \perp \begin{bmatrix} \boldsymbol{p}_{\mathrm{f}}^{\ell+1} \\ \boldsymbol{s}^{\ell+1} \end{bmatrix} \geq 0, \tag{15}$$

where $\boldsymbol{s}^{\ell+1} \in \Re^{n_c}$ is the vector of tangential sliding speeds at the contacts, $\boldsymbol{U} = \mathrm{diag}(\mu_1, \ldots, \mu_{n_c})$ is the diagonal matrix of friction coefficients and $\boldsymbol{E} = \mathrm{diag}(\boldsymbol{e}, \ldots, \boldsymbol{e})$ is the block diagonal matrix with $\boldsymbol{e}$ vectors on the main diagonal. Notice that in these complementarity conditions, we have defined the quantities $\boldsymbol{\rho}_{\mathrm{f}}^{\ell+1}$ and $\boldsymbol{\sigma}^{\ell+1}$ which will be used later when we construct the set of possible external impulses consistent with seating a part.

2.5 Full Time-Stepping Model

Equations (10,13,15) constitute a mixed LCP. It is mixed because of the appearance of an equation (the Newton-Euler equation) that is not an integral part of a complementarity relationship. This mixed LCP can be solved reliably and efficiently by the *path* algorithm [12] available through CPNet.org. However for our purposes, it will be useful to solve equation (10) for $\boldsymbol{\nu}^{\ell+1}$ and eliminate it, yielding a standard LCP with $\boldsymbol{w}$, $\boldsymbol{z}$, $\boldsymbol{B}$ and $\boldsymbol{b}$ given as follows:

$$0 \le \boldsymbol{w} = \begin{bmatrix} \boldsymbol{\rho}_{\mathrm{n}}^{\ell+1} \\ \boldsymbol{\rho}_{\mathrm{f}}^{\ell+1} \\ \boldsymbol{\sigma}^{\ell+1} \end{bmatrix} \perp \begin{bmatrix} \boldsymbol{p}_{\mathrm{n}}^{\ell+1} \\ \boldsymbol{p}_{\mathrm{f}}^{\ell+1} \\ \boldsymbol{s}^{\ell+1} \end{bmatrix} = \boldsymbol{z} \ge 0 \tag{16}$$

$$\boldsymbol{B} = \begin{bmatrix} \boldsymbol{W}_{\mathrm{n}}^{T} \boldsymbol{M}^{-1} \boldsymbol{W}_{\mathrm{n}} & \boldsymbol{W}_{\mathrm{n}}^{T} \boldsymbol{M}^{-1} \boldsymbol{W}_{\mathrm{f}} & 0 \\ \boldsymbol{W}_{\mathrm{f}}^{T} \boldsymbol{M}^{-1} \boldsymbol{W}_{\mathrm{n}} & \boldsymbol{W}_{\mathrm{f}}^{T} \boldsymbol{M}^{-1} \boldsymbol{W}_{\mathrm{f}} & \boldsymbol{E} \\ \boldsymbol{U} & -\boldsymbol{E}^{T} & 0 \end{bmatrix} \tag{17}$$

$$\boldsymbol{b} = \begin{bmatrix} \boldsymbol{W}_{\mathrm{n}}^{T}(\boldsymbol{\nu}^{\ell} + \boldsymbol{M}^{-1}\boldsymbol{p}_{\mathrm{ext}}) + \boldsymbol{\Psi}_{\mathrm{n}}^{\ell}/h \\ \boldsymbol{W}_{\mathrm{f}}^{T}(\boldsymbol{\nu}^{\ell} + \boldsymbol{M}^{-1}\boldsymbol{p}_{\mathrm{ext}}) \\ 0 \end{bmatrix}. \tag{18}$$

3 Part Seating

Since our objective is to determine an impulse to apply to the part to cause it to seat, it would be nice if it were possible to determine a set of inequalities in $\boldsymbol{p}_{\mathrm{ext}}$ satisfying the conditions of part seating. To do this, we first rearrange the LCP defined above as follows:

$$\begin{bmatrix} \boldsymbol{I} & -\boldsymbol{B} \end{bmatrix} \begin{bmatrix} \boldsymbol{w} \\ \boldsymbol{z} \end{bmatrix} = \boldsymbol{P}\boldsymbol{p}_{\mathrm{ext}} + \boldsymbol{a} \tag{19}$$

$$0 \le \boldsymbol{w} \perp \boldsymbol{z} \ge 0, \tag{20}$$

where $\boldsymbol{P}$ and $\boldsymbol{a}$ are defined as follows:

$$\boldsymbol{P} = \begin{bmatrix} \boldsymbol{W}_{\mathrm{n}}^{T} \boldsymbol{M}^{-1} \\ \boldsymbol{W}_{\mathrm{f}}^{T} \boldsymbol{M}^{-1} \\ 0 \end{bmatrix} \qquad \boldsymbol{a} = \begin{bmatrix} \boldsymbol{W}_{\mathrm{n}}^{T} \boldsymbol{\nu}^{\ell} + \boldsymbol{\Psi}^{\ell}/h \\ \boldsymbol{W}_{\mathrm{f}}^{T} \boldsymbol{\nu}^{\ell} \\ 0 \end{bmatrix}.$$

Notice that if one can determine in advance which complementary variables will be zero, the remaining will be nonnegative and the LCP will reduce to a system of linear inequalities in $\boldsymbol{p}_{\mathrm{ext}}$, as desired. We exploit this idea below.

By definition, a part is seated if all intended contacts are achieved. This is equivalent to requiring that all the contact gaps are equal to zero at time $t_{\ell+1}$, *i.e.*, $\mathbf{\Psi}_{\mathrm{n}}^{\ell+1} = 0$. Also taking into account that for any well-designed fixture $\boldsymbol{W}_{\mathrm{n}}^{-1}$ will exist [13], then the requirement of part seating completely specifies the generalized velocity of the part at the end of the time step:

$$\boldsymbol{\nu}^{\ell+1} = -\boldsymbol{W}_{\mathrm{n}}^{-T}\mathbf{\Psi}_{\mathrm{n}}^{\ell+1}/h.$$

Now, consider the first row of condition (15). Recall that $\boldsymbol{W}_{\mathrm{f}}^{T}$ projects the body velocity onto the positive and negative tangential directions at the contacts. The magnitudes of these projections are the sliding speeds (averaged over the time step) at the contacts. In typical part seating scenarios, each element of $\boldsymbol{s}^{\ell+1}$ will be strictly positive.

Consider now the second row of condition (15). When $\boldsymbol{s}^{\ell+1}$ is strictly positive, the left-hand inequality must be satisfied by equality. The only way this is possible is for a friction impulse to be delivered, *i.e.,* at least one of $(p_{if})_1$ and $(p_{if})_2$ to be nonzero. Returning to the first row of condition (15), we see that when $s_i^{\ell+1}$ is positive, only one of the two inequalities involving $s_i^{\ell+1}$ on the left-hand side of condition (15) can be satisfied by equality. Therefore, one must be satisfied by equality and the other one by strict inequality. Causing one of p_{if_1} and p_{if_2} to be zero. The value of the other one must have the value $\mu_i p_{in}^{\ell+1}$.

While the complementarity conditions enforce Coulomb's Law, it is easier to choose the active and inactive friction impulse magnitudes by computing the tangential velocity at the contact points directly as:

$$\boldsymbol{v}_{\mathrm{t}}^{\ell+1} = -\boldsymbol{W}_{\mathrm{t}}^{T}\boldsymbol{W}_{\mathrm{n}}^{-T}\mathbf{\Psi}_{\mathrm{n}}^{\ell}/h.$$

Each of the elements of $\boldsymbol{v}_{\mathrm{t}}^{\ell+1}$ is the magnitude of the sliding velocity at the contact in the $\hat{\boldsymbol{t}}$ direction at each contact. If the sliding velocity at contact i is positive in the $\hat{\boldsymbol{t}}_i$ direction (*i.e.*, $v_{it} > 0$) then the friction impulse must be in the opposite direction, and so $p_{if_1} = 0$ and $p_{if_2} \geq 0$. If v_{it} is less than zero, then we know that $p_{if_1} \geq 0$ and $p_{if_2} = 0$

In summary, all gaps are set to zero, all elements of $\boldsymbol{\sigma}^{\ell+1}$ are set to zero, the half of the friction impulse magnitudes that would add energy to the system are set to zero, and the elements of $\boldsymbol{\rho}_{if}$ corresponding to dissipative friction impulses are set to zero. After this is done, the LCP (19,20) reduces to a square system (of size $4n_c$) of linear inequalities in $\boldsymbol{p}_{\mathrm{ext}}$ as follows:

$$\boldsymbol{K}\boldsymbol{y} = \boldsymbol{P}\boldsymbol{p}_{\mathrm{ext}} + \boldsymbol{a} \tag{21}$$

$$\boldsymbol{y} \geq 0, \tag{22}$$

where $\boldsymbol{y}$ is obtained from $\begin{bmatrix} \boldsymbol{w} \\ \boldsymbol{z} \end{bmatrix}$ by removing that elements that have been set to zero (half of them) and $\boldsymbol{K}$ is obtained from $\begin{bmatrix} \boldsymbol{I} & -\boldsymbol{B} \end{bmatrix}$ by removing the corresponding columns. The following example illustrates the approach. Equations (21) and (22) define the set of all impulses consistent with part seating.

3.1 Example 1

Let us now revisit the initial problem of moving a point of unit mass with initial coordinates (x, y) into a corner (see Figure 1). Again, assume that the point begins at rest in a contact-free position $(x, y > 0)$ with the objective of finding all external impulses $\boldsymbol{p}_{\text{ext}}$ that place the point in the corner, touching both the x- and y-axes, at the end of the current time step, h.

The defining quantities of the discrete-time dynamic in equation (16) are given as follows:

$$\boldsymbol{q}^l = \begin{bmatrix} x \\ y \end{bmatrix} > 0 \quad \boldsymbol{\Psi}_{\text{n}}^\ell = \begin{bmatrix} x \\ y \end{bmatrix} \quad h = 1 \quad \boldsymbol{\nu}^l = \begin{bmatrix} 0 \\ 0 \end{bmatrix} \quad \boldsymbol{M} = \begin{bmatrix} 1 & 0 \\ 0 & 1 \end{bmatrix}$$

$$\boldsymbol{W}_n = \begin{bmatrix} 1 & 0 \\ 0 & 1 \end{bmatrix} \quad \boldsymbol{W}_f = \begin{bmatrix} 0 & 0 & -1 & 1 \\ 1 & -1 & 0 & 0 \end{bmatrix} \quad \boldsymbol{U} = \begin{bmatrix} \mu_1 & 0 \\ 0 & \mu_2 \end{bmatrix} \quad \boldsymbol{E}^T = \begin{bmatrix} 1 & 1 & 0 & 0 \\ 0 & 0 & 1 & 1 \end{bmatrix}.$$

Additional values imposed by the requirement that the point move to the corner in a single time step are:

$$\boldsymbol{q}^{l+1} = \begin{bmatrix} 0 \\ 0 \end{bmatrix} \quad \boldsymbol{\Psi}_{\text{n}}^{\ell+1} = \begin{bmatrix} 0 \\ 0 \end{bmatrix}$$

Since the point is to be moved into the corner, both rows of $\boldsymbol{\rho}_n$ in equation (16) must be strictly zero. This implies that the normal impulses applied to the point over the time step may be strictly positive, which is consistent with the fact that when contact is achieved, an impulse must be applied to by the constraint surfaces to the point to prevent penetration. Solving these equations for $\boldsymbol{\nu}^{l+1}$ yields:

$$\boldsymbol{\nu}^{l+1} = \begin{bmatrix} -\psi_1^l/h \\ -\psi_2^l/h \end{bmatrix}$$

In other words, the x- and y-component speeds of the point at the end of the current time step must be just large enough to reach the corresponding barriers. Note that for large impulses, the speeds could be very high, but the average speeds over the time step will be as computed, since at the end of the time step we must have contact with both axes.

Next consider the friction direction complementarity conditions for contact with the x-axis. Substituting the assumed values into the first two rows of $\boldsymbol{\rho}_f$ in equation (16) yields:

$$\text{sliding left:} \quad 0 \leq \psi_1^l + s_1^{l+1} \perp (p_{1f})_1^{l+1} \geq 0 \tag{23}$$

$$\text{sliding right:} \quad 0 \leq -\psi_2^l + s_2^{l+1} \perp (p_{1f})_2^{l+1} \geq 0 \tag{24}$$

where the friction impulses $(p_{1f})_1^{l+1}$ and $(p_{1f})_2^{l+1}$ act in the negative and positive x-directions respectively. Notice that the left-hand sides of equations (23) and (24)

are equivalent to $s_2^{l+1} \geq \psi_2^l$. Therefore s_2^{l+1} is strictly positive implying (through condition (23)) that the $(p_{1f})_1^{l+1} = 0$. Since the gap to the y-axis must close during the time step, the motion of the point must have a component to the left, so the left-pointing friction force must be zero. Only the right-pointing component $(p_{1f})_2^{l+1}$ can be positive.

Using the above results, the second row of $\boldsymbol{\sigma}$ in complementarity equation (16) (which applies to the contact on the x-axis) becomes:

$$0 \leq \mu_1 p_{1n}^{l+1} - (p_{1f})_2^{l+1} \quad \perp \quad s_2^{l+1} \geq 0. \tag{25}$$

Since s_2^{l+1} is strictly positive, the left side of the condition must be zero, yielding that the friction impulse is μ_1 times the normal impulse, *i.e.*, $(p_{1f})_2^{l+1} = \mu_1 p_{1n}^{l+1}$. Results for contact with the y-axis are analogous.

We are now in a position to achieve our original objective of determining the set of all $\boldsymbol{p}_{\text{ext}}$ that drive the point into the corner. The above analysis identified certain unknowns as zero and fixed values for others. Substituting those values into equation (10) yields:

$$\begin{bmatrix} p_{\text{ext},x}^{l+1} \\ p_{\text{ext},y}^{l+1} \end{bmatrix} = \begin{bmatrix} -\mu_1 & -1 \\ -1 & -\mu_2 \end{bmatrix} \begin{bmatrix} p_{1n}^{l+1} \\ p_{2n}^{l+1} \end{bmatrix} + \begin{bmatrix} \psi_1^l \\ \psi_2^l \end{bmatrix} \tag{26}$$

where recall that $p_{1n}^{l+1}, p_{2n}^{l+1} \geq 0$. Equation (26) is nearly in the form of a polyhedral convex cone. Only the nonzero initial gaps prevent this. However, one can see that the effect of the gaps is to translate the cone by gap vector as shown in Figure 2.
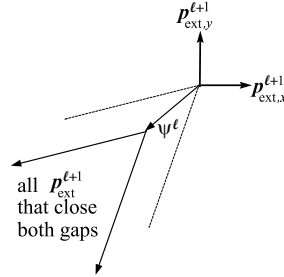
Fig. 2. Convex cone of external impulses that place the point in the corner at the end of a time step of length one unit with initial gaps given by the vector ψ^l.

3.2 Example 2

Figure 3 shows a rectangular part that is to be placed in contact with three fixels. The part begins at rest near, but not in contact with, the fixels. When in contact with all three fixels, the body-fixed frame will coincide with the inertial (x, y)-frame. Our
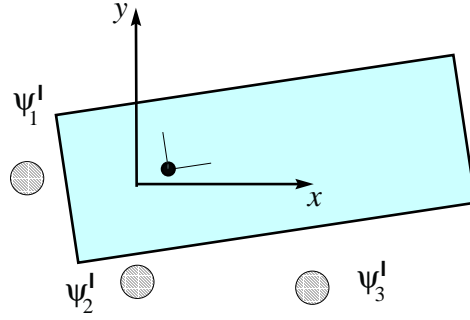
Fig. 3. A planar part near its seated configuration.

goal is to identify the set of external impulses that achieve all three contacts without specifying anything about the order of contact achievement.

We set $h = 1$ and define the additional quantities as follows:

$$\boldsymbol{q}^{\ell} = \begin{bmatrix} x \\ y \\ \theta \end{bmatrix} \quad \boldsymbol{\Psi}_{\mathrm{n}}^{\ell} = \begin{bmatrix} 0.10 \\ 0.05 \\ 0.20 \end{bmatrix} \quad \boldsymbol{\nu}^{\ell} = \begin{bmatrix} 0 \\ 0 \\ 0 \end{bmatrix} \quad \boldsymbol{M} = \begin{bmatrix} 1 & 0 & 0 \\ 0 & 1 & 0 \\ 0 & 0 & 1 \end{bmatrix} \quad \boldsymbol{W}_{\mathrm{n}} = \begin{bmatrix} 1 & 0 & 0 \\ 0 & 1 & 1 \\ 0 & 0 & 1 \end{bmatrix}$$

$$\boldsymbol{W}_{\mathrm{f}} = \begin{bmatrix} 0 & 0 & -1 & 1 & -1 & 1 \\ 1 & -1 & 0 & 0 & 0 & 0 \\ -1 & 1 & -1 & 1 & -1 & 1 \end{bmatrix} \quad \boldsymbol{U} = \begin{bmatrix} \mu_1 & 0 & 0 \\ 0 & \mu_2 & 0 \\ 0 & 0 & \mu_3 \end{bmatrix} \quad \boldsymbol{E}^T = \begin{bmatrix} 1 & 1 & 0 & 0 & 0 & 0 \\ 0 & 0 & 1 & 1 & 0 & 0 \\ 0 & 0 & 0 & 0 & 1 & 1 \end{bmatrix}.$$

We now have all the data required to construct equations (19) and (20).

$$\boldsymbol{B} = \begin{bmatrix} 1 & 0 & 0 & 0 & 0 & -1 & 1 & -1 & 1 & 0 & 0 & 0 \\ 0 & 1 & 1 & 1 & -1 & 0 & 0 & 0 & 0 & 0 & 0 & 0 \\ 0 & 1 & 2 & 0 & 0 & -1 & 1 & -1 & 1 & 0 & 0 & 0 \\ 0 & 1 & 0 & 2 & -2 & 1 & -1 & 1 & -1 & 1 & 0 & 0 \\ 0 & -1 & 0 & -2 & 2 & -1 & 1 & -1 & 1 & 1 & 0 & 0 \\ -1 & 0 & -1 & 1 & -1 & 2 & -2 & 2 & -2 & 0 & 1 & 0 \\ 1 & 0 & 1 & -1 & 1 & -2 & 2 & -2 & 2 & 0 & 1 & 0 \\ -1 & 0 & -1 & 1 & -1 & 2 & -2 & 2 & -2 & 0 & 0 & 1 \\ 1 & 0 & 1 & -1 & 1 & -2 & 2 & -2 & 2 & 0 & 0 & 1 \\ \mu_1 & 0 & 0 & -1 & -1 & 0 & 0 & 0 & 0 & 0 & 0 & 0 \\ 0 & \mu_2 & 0 & 0 & 0 & -1 & -1 & 0 & 0 & 0 & 0 & 0 \\ 0 & 0 & \mu_3 & 0 & 0 & 0 & 0 & -1 & -1 & 0 & 0 & 0 \end{bmatrix} \quad \boldsymbol{P} = \begin{bmatrix} 1 & 0 & 0 \\ 0 & 1 & 0 \\ 0 & 1 & 1 \\ 0 & 1 & -1 \\ 0 & -1 & 1 \\ -1 & 0 & -1 \\ 1 & 0 & 1 \\ -1 & 0 & -1 \\ 1 & 0 & 1 \\ 0 & 0 & 0 \\ 0 & 0 & 0 \\ 0 & 0 & 0 \end{bmatrix} \quad \boldsymbol{a} = \begin{bmatrix} 0.1 \\ 0.05 \\ 0.2 \\ 0 \\ 0 \\ 0 \\ 0 \\ 0 \\ 0 \\ 0 \\ 0 \\ 0 \end{bmatrix}$$

Setting the gaps to zero at the end of the time step gives:

$$\boldsymbol{\Psi}_{\mathrm{n}}^{\ell+1} = 0 \quad \Rightarrow \quad \boldsymbol{p}_{\mathrm{n}}^{\ell+1} \geq 0$$

Zero gaps also allows us to solve for $s^{\ell+1}$. The signs of the elements of $s^{\ell+1}$ allow us to determine the signs of the elements of $\sigma^{\ell+1}$, and less directly, the signs of $\rho_f^{\ell+1}$ and $p_f^{\ell+1}$. We obtain:

$$s^{\ell+1} = v_t^{\ell+1} = \begin{bmatrix} 0.10 \\ 0.25 \\ 0.25 \end{bmatrix} \quad \Rightarrow \quad \sigma^{\ell+1} = 0.$$

Further, we find:

$$s^{\ell+1} > 0 \quad \Rightarrow \quad \begin{cases} (p_{1f})_1^{\ell+1} = 0, & (p_{1f})_2^{\ell+1} = \mu_1 p_{1n}^{\ell+1} \geq 0 \\ (p_{2f})_1^{\ell+1} = 0, & (p_{2f})_2^{\ell+1} = \mu_2 p_{2n}^{\ell+1} \geq 0 \\ (p_{3f})_1^{\ell+1} = 0, & (p_{3f})_2^{\ell+1} = \mu_3 p_{3n}^{\ell+1} \geq 0 \end{cases} \quad \begin{matrix} (\rho_{1f})_2^{\ell+1} = 0 \\ (\rho_{2f})_2^{\ell+1} = 0 \\ (\rho_{3f})_2^{\ell+1} = 0 \end{matrix}$$

Finally we obtain the following definitions of K and y:

$$K = \begin{bmatrix} 0 & 0 & 0 & -1 & 0 & 0 & 0 & -1 & -1 & 0 & 0 & 0 \\ 0 & 0 & 0 & 0 & -1 & -1 & 1 & 0 & 0 & 0 & 0 & 0 \\ 0 & 0 & 0 & 0 & -1 & -2 & 0 & -1 & -1 & 0 & 0 & 0 \\ 1 & 0 & 0 & 0 & -1 & 0 & 2 & 1 & 1 & -1 & 0 & 0 \\ 0 & 0 & 0 & 0 & 1 & 0 & -2 & -1 & -1 & -1 & 0 & 0 \\ 0 & 1 & 0 & 1 & 0 & 1 & 1 & 2 & 2 & 0 & -1 & 0 \\ 0 & 0 & 0 & -1 & 0 & -1 & -1 & -2 & -2 & 0 & -1 & 0 \\ 0 & 0 & 1 & 1 & 0 & 1 & 1 & 2 & 2 & 0 & 0 & -1 \\ 0 & 0 & 0 & -1 & 0 & -1 & -1 & -2 & -2 & 0 & 0 & -1 \\ 0 & 0 & 0 & -\mu_1 & 0 & 0 & 1 & 0 & 0 & 0 & 0 & 0 \\ 0 & 0 & 0 & 0 & -\mu_2 & 0 & 0 & 1 & 0 & 0 & 0 & 0 \\ 0 & 0 & 0 & 0 & 0 & -\mu_3 & 0 & 0 & 1 & 0 & 0 & 0 \end{bmatrix} \qquad y = \begin{bmatrix} (\rho_{1f})_1^{\ell+1} \\ (\rho_{2f})_1^{\ell+1} \\ (\rho_{3f})_1^{\ell+1} \\ p_{1n}^{\ell+1} \\ p_{2n}^{\ell+1} \\ p_{3n}^{\ell+1} \\ (p_{1f})_2^{\ell+1} \\ (p_{2f})_2^{\ell+1} \\ (p_{3f})_2^{\ell+1} \\ s_1^{\ell+1} \\ s_2^{\ell+1} \\ s_3^{\ell+1} \end{bmatrix}$$

Letting $\mu_i = 0.1$ for all i, we can now test if a particular external impulse p_{ext} lies within the set of external impulses that accomplish the seating operation by testing if:

$$(K^{-1}P)p_{ext} \geq -K^{-1}a. \tag{27}$$

Using our example we see that one possible external impulse is:

$$p_{ext} = [-1 \ -1 \ -1]^T$$

We can easily verify this value using inequality (27).

$$
(\boldsymbol{K}^{-1}\boldsymbol{P})\boldsymbol{p}_{\text{ext}} =
\begin{bmatrix}
0.0000 \\
0.0000 \\
0.0000 \\
0.8911 \\
0.2871 \\
0.8020 \\
0.0891 \\
0.0287 \\
0.0802 \\
0.0000 \\
0.0000 \\
0.0000
\end{bmatrix}
\geq
\begin{bmatrix}
-0.2000 \\
-0.5000 \\
-0.5000 \\
0.0941 \\
-0.0752 \\
0.1347 \\
0.0094 \\
-0.0075 \\
0.0135 \\
-0.1000 \\
-0.2500 \\
-0.2500
\end{bmatrix}
= -\boldsymbol{K}^{-1}\boldsymbol{a}
$$

Since inequality (27) is satisfied for the example with the given $\boldsymbol{p}_{\text{ext}}$, this implies that an external impulse pushing the object directly towards the origin while applying a clockwise moment will seat the part, which we would have expected.

3.3 Stability

Applying an impulse in the polytope defined by equation (21) will seat the part as required, but it does not guarantee that the part will remain seated if a wrench in the direction of the impulse is continuously applied to the part. To ensure seating stability, one can perform an instantaneous analysis to obtain the wrench cone that provides strong stability once the part is seated [7]. Multiplying this cone by the time step h yields an impulse cone. The intersection of this cone and set derived above is the set of impulses that can be applied to both seat the part and maintain the contacts.

4 The Pushing Region

Now that we have a representation of the set of impulses consistent with part seating, we would like to find points on the boundary of the part where such impulses can be generated by contact. Identifying all such boundary points defines a *pushing region*, where one can seat the part simply by pushing at any point in the region.

One straight forward, but computationally intensive, approach for determining the pushing region is point sampling of the boundary. For a given point and coefficient of friction, one can determine the cone of wrenches that could be produced by contact. The set of possible (generalized) impulses that can be generated through contact is the wrench cone scaled by the time step and the time-average wrench magnitude. Therefore, the contact wrench cone and contact impulse cones are identical. For the

given point to be in the pushing region, every ray of the contact wrench cone must intersect the set of part seating impulses.

Identifying the pushing region by point sampling and testing is not desirable. Not only does it require a large number of tests to be done for a pair of points in the pushing region, but the status of the points between them is not known. In order to solve this problem, we have developed a method to test finite-length boundary segments. This analysis first places conservative bounds on all wrenches that can be produced via contact with the segment. If this entire conservative set satisfies the test, then the segment is part of the pushing region. When the entire conservative set fails the test, the segment is excluded from the pushing region. Otherwise, the segment can be divided into smaller pieces and testing repeated.

In Figure 4(b), a segment of the boundary of a part is shown in a rectangle that contains the segment. Also shown are extreme contact force directions for contact anywhere on the boundary segment under the assumption of no friction. The conservative set of wrenches implied by the bounding box and the contact force directions defines a set of wrenches such that for each wrench, the line of action is parallel to one possible force direction vector and intersects the bounding box. In practice, the bounding box will be closer in size to the boundary segment. Further, one can add friction to the analysis by simply replacing the boundary normal direction vectors shown, by a cone of normal directions dictated by the coefficient of friction.

(a) Part   (b) Curve Segment
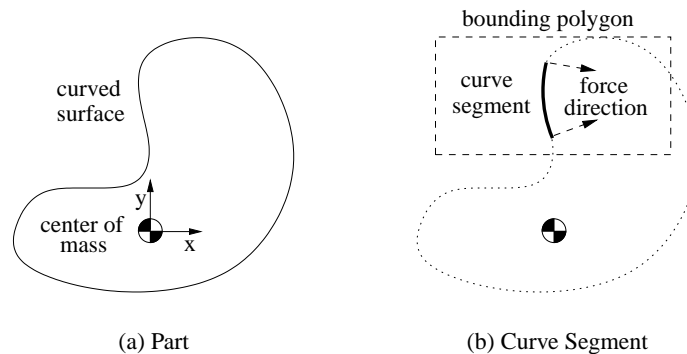
Fig. 4. On the left is curved 2D part whose boundary is to be analyzed to find a pushing region. On the right is a curve segment, a polygon containing the segment, and the unit force direction vectors at the endpoints.

4.1 Assumptions

To calculate a conservative set of wrenches bounding those that can be generated through contact with a boundary segment of a part, we make the following assumptions:

1. The boundary of the part can be partitioned into curve segments, where each segment s is defined parametrically by:

$$s(\tau) = (x(\tau), y(\tau)), \quad \tau \in [0, 1]. \tag{28}$$

2. We can bound all points of s within a simple polygon composed of vertices $(p_1, p_2, \ldots, p_n)$.

3. For each point it is possible to calculate bounds for the direction θ of the inward force vector $\hat{\boldsymbol{d}}$ (in the frictionless case $\hat{\boldsymbol{d}} = \hat{\boldsymbol{n}}$):

$$\theta_{start} \leq \theta(\tau) \leq \theta_{end} \tag{29}$$

4.2 Variables

For a single point and force direction we construct a position vector $\boldsymbol{r}$ as well as an inward facing force direction vector $\hat{\boldsymbol{d}}$. The wrench that can be exerted by pushing at the point $\boldsymbol{r}$ in the direction of $\hat{\boldsymbol{d}}$ with magnitude λ_{n} is:

$$\boldsymbol{w} = \begin{bmatrix} d_x \\ d_y \\ X \end{bmatrix} \lambda_{\mathrm{n}}. \tag{30}$$

where d_x and d_y are the components of $\hat{\boldsymbol{d}}$ and $X = \boldsymbol{r} \otimes \hat{\boldsymbol{d}}$ is the moment of the direction vector with respect to the center of mass of the part. We also denote the direction of $\boldsymbol{r}$ by ϕ.

4.3 Wrench Bounds for a Curve

It is easy to determine bounds on the x- and y-components of the unit normals of a boundary segment, but bounding the moment of the contact force is more difficult, because it depends on both the force direction and the position of the line of action. The moment of the contact force, when friction is present and the force direction is uncertain, is a nonlinear set-valued function of the variable τ, which makes it difficult to compute tight analytic bounds on the possible contact wrenches of a given boundary segment. In order to avoid the difficulties of determining X analytically, we instead generate conservative bounds.

The proofs to support our construction of wrench bounds are contained in a recent technical report [14]; the following is a summary of those results. We first bound all possible force directions of a segment by $[\theta_{start}, \theta_{end}]$. We then examine the values of X produced by θ_{start} and θ_{end} at each and every vertex of the bounding polygon. If one of the values of θ in the range $[\theta_{start}, \theta_{end}]$ is equal to $\phi \pm \pi$ (*i.e.* $\hat{\boldsymbol{d}} \perp \boldsymbol{r}$), then we also calculate X for that value of θ as well (as shown in Fig. 5). Next, we examine all of the values of X to find X_{min} and X_{max}. If we allow λ_{n} to take on any non-negative value, then we create a four sided convex polyhedral cone in wrench space.
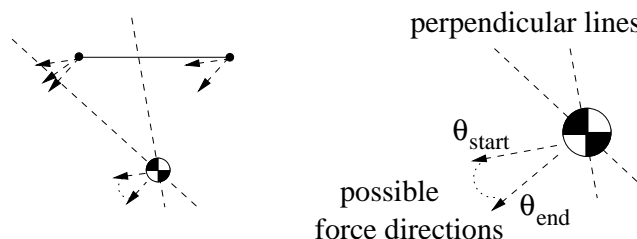
Fig. 5. A third value of θ must be tested for the left endpoint because the extra θ value is perpendicular to ϕ and within $[\theta_{start}, \theta_{end}]$.

Figures 6(a) shows a boundary segments of a part in relation to its center of mass. The boundary is represented by cubic B-splines, whose control points are also shown. The curve segment defined by the leftmost four control points is shown dark (blue). The polygon defined by these points and range of contact force directions with $\mu = 0.2$ were used to generate a conservative wrench cone. This wrench cone is guaranteed to contain all contact wrenches that could be generated through contact with the segment. Both the conservative wrench cone and the exact wrench cone under frictionless assumption are shown mapped onto the unit sphere in Figure 6(b). The same is done for the light (red) segment defined by all but the upper-most control point.

5   Using the Set of Bounded Wrenches

The last step is to determine the pushing region on the boundary of the part. To do this, one breaks the boundary into a number of segments, computes their bounding wrench cones, and intersects them with the set of seating impulses determined in section 3. This intersection, however, requires some explanation. Recall that the objective is to apply an impulse to the object by pushing on the object's boundary. Pushing on a given point on the boundary of the part can seat the part if the ray of the corresponding wrench intersects the set of seating impulses. To actually seat the part, one must push with the proper force magnitude and length of time, so that an impulse in the part seating set is applied.

Given the preceding discussion, when building the pushing region, the ideal boundary segment is one for which every ray in the conservative cone intersects the seating set. It is even more desirable if the intersection is a half line, so that the magnitude and time of the push does not have to be precisely controlled.

Nonetheless, the pushing region can be constructed by identifying segments for which all contained wrench directions intersect the seating impulse cone. These segments are included in the pushing region. Segments whose cones do not intersect the seating impulse set are discarded. The remaining segments are divided into shorter segments which are tested in the same way. Segment division continues recursively until a given resolution is reached, or until a large enough pushing region has been identified.
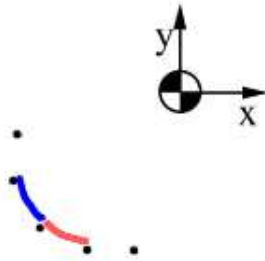
(a) Boundary
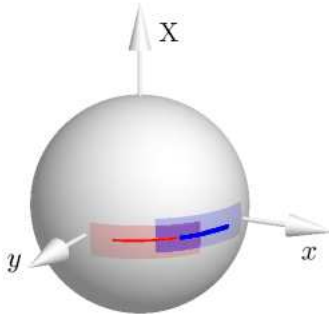
(b) Wrenches

Fig. 6. Two curve segments defining a portion of a part's boundary with conservative bounds and frictionless point sampled results mapped to the sphere of unit wrenches.

6   Summary and Future Work

Given a fixed part and a moveable part near its fixtured configuration, we have developed two basic analytical tools for planning dynamic sensorless part seating/insertion tasks. Based on a dynamic model of rigid bodies in unilateral contact, we showed how one can identify the polytope of impulses consistent with seating the part in one time step. This can be used in conjunction with previous instantaneous analysis to find the set of impulses that can be applied to achieve the required contacts and maintain them. The second tool computes a conservative wrench cone that contains all wrenches that can be applied through contact at any point along a (nonzero) finite-length boundary segment of a planar part. Segments can then be identified as in or

out of the pushing region or partially in. Those that are partially in can be recursively partitioned and tested until a specified resolution or until the size of the pushing region is large enough to reliably perform the task.

Several open questions remain. The most important of these is related to solution nonuniqueness. The seating impulse polytope is all wrenches *consistent* with seating. It is possible that some of these wrenches are consistent with part motions that do *not* result in seating. It is not known if any such wrenches exists for the special case of the part seating problem studied here. If they do, it is likely that it will be computationally expensive to identify them exactly and remove them from the seating impulse set. However, it must be done if one is to use our tools to plan robust part seating strategies.

Other interesting lines of continued research include the extension to three-dimensional part-seating problems and multi-push strategies.

Acknowledgments

References

1. Mason, M.T.: Mechanics of robotic manipulation. MIT Press (2001)
2. Trinkle, J., Hunter, J.J.: A framework for planning dexterous manipulation. In: Proceedings, IEEE International Conference on Robotics and Automation. (1991) 1245–1251
3. Trinkle, J., Zeng, D.: Prediction of the quasistatic planar motion of a contacted rigid body. IEEE Transactions on Robotics and Automation **11** (1995) 229–246
4. Erdmann, M.A.: On motion planning with uncertainty. Master's thesis, MIT Department of Electrical Engineering and Computer Science (1984)
5. Brost, R.C.: Analysis and Planning of Planar Manipulation Tasks. PhD thesis, Carnegie Mellon University School of Computer Science (1991)
6. Farahat, A., Stiller, P., Trinkle, J.: On the algebraic geometry of contact formation cells for systems of polygons. In: Proceedings, Workshop on Algorithmic Foundations of Robotics, A.K. Peters, Boston, MA (1994) 477–494
7. Balkcom, D., Trinkle, J.: Computing wrench cones for planar rigid body contact tasks. International Journal of Robotics Research **21** (2002) 1053–1066
8. Trinkle, J., Pang, J., Sudarsky, S., Lo, G.: On dynamic multi-rigid-body contact problems with coulomb friction. Zeitschrift für Angewandte Mathematik und Mechanik **77** (1997) 267–279
9. Stewart, D., Trinkle, J.: An implicit time-stepping scheme for rigid body dynamics with inelastic collisions and coulomb friction. International Journal of Numerical Methods in Engineering **39** (1996) 2673–2691
10. Stewart, D., Trinkle, J.: An implicit time-stepping scheme for rigid body dynamics with coulomb friction. In: Proceedings, IEEE International Conference on Robotics and Automation. (2000) 162–169
11. Cottle, R.W., Pang, J., Stone, R.E.: The Linear Complementarity Problem. Academic Press (1992)

12. Ferris, M.C., Munson, T.S.: Complementarity problems in GAMS and the PATH solver. Technical Report MP-TR-1998-12 (1998)
13. Asada, H., By, A.B.: Kinematics of workpart fixturing. In: Proceedings, IEEE International Conference on Robotics and Automation. (1985) 337–345
14. Egan, K., Berard, S., Trinkle, J.C.: Computing wrench bounds along a curved surface in 2d. Technical Report no. 04-06, Rensselaer Polytechnic Institute (2004)